Nanoscale

Accepted Manuscript

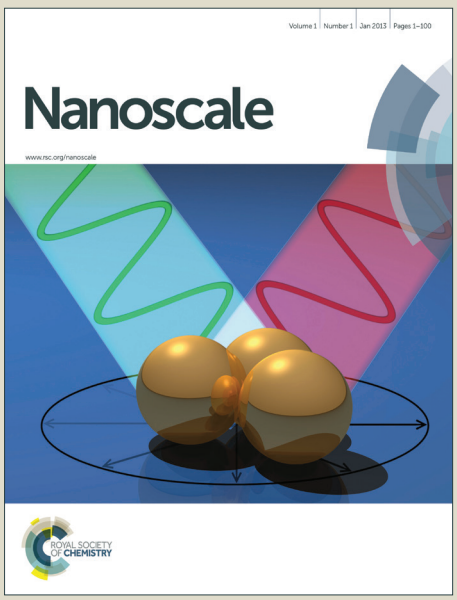

ROYAL SOCIETY OF CHEMISTRY

www.rsc.org/nanoscale

Journal Name

ARTICLE

An ultrastable conjugate of silver nanoparticle and protein formed through weak interactions

Received 00th January 20xx,
Accepted 00th January 20xx

DOI: 10.1039/x0xx00000x

www.rsc.org/

Varsha P. Brahmkhatri,[a,†] Kousik Chandra, [a,†] Abhinav Dubey[a,b] and Hanudatta S. Atreya[a,c]*

In recent years, silver nanoparticles (AgNPs) have attracted significant attention owing to their unique physicochemical, optical, conductive and antimicrobial properties One of the properties of AgNPs which is crucial for all applications is their stability. In the present study we unravel a mechanism through which silver nanoparticles are rendered ultrastable in an aqueous solution in complex with the protein ubiquitin (Ubq). This involves a dynamic and reversible association and dissociation of ubiquitin from the surface of AgNP. The exchange occurs at a rate much greater than 25 s^{-1} implying a residence time of < 40 ms for the protein. The AgNP-Ubq complex remains stable for months due to steric stabilization over a wide pH range compared to unconjugated AgNPs. NMR studies reveal that the protein molecules bind reversibly to AgNP with an approximate dissociation constant of 55 μM and undergo fast exchange. At pH > 4 the positively charged surface of the protein comes in contact with the citrate capped AgNP surface. Further, NMR relaxation-based experiments suggest that in addition to the dynamic exchange, a conformational rearrangement of the protein takes place upon binding to AgNP. The ultrastability of the AgNP-Ubq complex was found to be useful for its anti-microbial activity, which allowed the recycling of this complex multiple times without loss of stability. Taken together, the study provides new insights into the mechanism of protein-silver nanoparticle interactions and opens up new avenues for its application in a wide range of systems.

Introduction

Among the various nanomaterials silver nanoparticles (AgNPs) have attracted a large attention due to their novel physicochemical, optical, conductive and antimicrobial properties[1-3]. AgNPs represent one of the most commercially important groups of nanomaterials due to their wide range of applications in almost every field of nanotechnology and nanomedicine [4, 5, 6, 7, 8, 9, 10]. However, unlike gold the susceptibility of silver to oxidation has restricted the development of important silver-based nanomaterials. A persistent focus has been to develop AgNPs that are inert or have long-term stability. Significant efforts have been made to improve the stability of AgNPs by employing various capping agents, ionic surfactants (such as sodium dodecyl sulphate and cetyltrimethylammonium bromide[11]), organic ligands including thiolates [12, 13], polymers [14-16] and natural biomaterials [16]. In addition many silver based antibacterial nanocomposites based on graphene oxide and titania have also been reported [17-19].

Colloidal stability is essential to AgNP-based nanoproducts because it affects most of the important properties associated with their performance namely their size, shape, and surface area [20]. Consequently, a number of studies have focused on aggregation and dissolution of AgNPs in cell culture media, in natural water or in the formulation of consumer products [20-22]. Notwithstanding these efforts, a mechanistic insight into the interaction and stability of AgNPs with different ligands, especially biomolecules in general and proteins in particular is incomplete. The AgNPs have two structural constituents that can contribute towards their interaction and stability with biomolecules, the metal core surface and the citrate ligands. One fundamental complication yet to be investigated is the

[a] NMR Research Centre, Indian Institute of Science, Bangalore-560012, India.
[b] IISc Mathematics Initiative, Indian Institute of Science, Bangalore-560012, India.
[c] NMR Research Centre and Solid State Structural Chemistry Unit, Indian Institute of Science, Bangalore-560012, India
† Contributed equally to this work
*Author for Correspondence

Electronic Supplementary Information (ESI) available: [details of any supplementary information available should be included here]. See DOI: 10.1039/x0xx00000x

mode of protein nanoparticle interactions, which has several possibilities such as the binding of the protein to the metal core either directly or through the citrate capping or both.

Protein-nanoparticle interactions result in formation of a dynamic nanoparticle-protein corona [23-25]. The protein corona may affect cellular uptake, inflammation, accumulation, degradation and clearance of the nanoparticles[25, 26]. So far the nanoparticle-protein corona has been explored experimentally using circular dichroism, fluorescence, infrared spectroscopy and various other methods that are limited to monitor changes in the secondary structure of proteins [27-30]. Complete details of the structural changes at an atomic level occurring in the protein upon binding to nanoparticles remains a challenge. Nuclear magnetic resonance (NMR) is a powerful tool for such studies due to its high sensitivity and resolution to protein–ligand interactions [31, 32]. NMR has been used to characterize protein-nanoparticle interactions using various multidimensional experiments[29, 33-36].

In the present study, using NMR spectroscopy and other techniques we have probed in detail the mechanism of protein-AgNP interactions which render the AgNPs ultrastable. The study reveals a mechanism which involves a relatively fast and reversible association-dissociation of human ubiquitin (dynamic exchange) from the surface of AgNP. The AgNP-Ubq complex remains stable for months over a wide pH range short time. The techniques employed in addition to NMR include UV-Visible spectroscopy, dynamic light scattering (DLS), zeta potential measurements and transmission electron microscopy (TEM). NMR studies suggest that the protein molecules bind to the AgNP with an approximate dissociation constant of 55 μM coming under the fast exchange regime at the magnetic field strength of 18.8 T used in the study. At pH > 4 the positively charged surface of the protein comes in contact with the AgNP surface, while the negatively charged surface faces the dispersion medium. Further, NMR relaxation-based experiments suggest that in addition to the fast exchange, a structural reorientation/ rearrangement of the protein takes place upon binding. The ultrastability of the AgNP-Ubq complex was found to be useful for its anti-microbial activity, which allowed the recycling of this complex multiple times without loss of stability unlike the uncomplexed AgNPs.

Materials and Methods

UV-visible spectroscopy

To confirm the binding of Ubq to AgNP and to study the stability of AgNP-Ubq conjugate UV-visible spectra were recorded on a Shimadzu UV-1800 UV-VIS Spectrophotometer. The final concentration of AgNP was 2.8 nM, which was mixed with 50 μM unlabelled ubiquitin in water to form the complex and incubated for few hours before starting the measurement. The stability of AgNP and AgNP-Ubq were measured in 50 mM Phosphate-buffer with 50 mM NaCl at different pH from 3-11. Stability profiles were plotted using absorbance values at respective absorption maxima for AgNPs and AgNP-Ubq as a function of time.

Dynamic light scattering (DLS) and Zeta potential measurement

The hydrodynamic radii and zeta potential of AgNPs, UBQ and AgNP-Ubq were measured using Nanozetasizer machine (Brookhaven Zeta PALS). Samples for DLS and zeta potential were prepared in 50 mM phosphate buffer or water as required. The AgNPs and Ubq were taken in the range of 3-6 nM and 25-50 μM, respectively. Further the zeta potential of AgNPs, UBQ and AgNP-Ubq was measured at different pH in 50 mM Phosphate-buffer containing 50 mM NaCl.

Transmission electron microscopy (TEM)

The TEM images were obtained with a Technai T-20 machine at an operating voltage of 200 kV. AgNPs (5.6 nM) were incubated at room temperature in deionized water (18 MΩ-cm) at neutral pH with unlabelled ubiquitin (50 μM), pipetted on a copper grid and dried overnight at room temperature in a desiccator.

Scanning electron microscopy (SEM)

To observe the morphological variations of bacterial cells treated with AgNPs and AgNP-Ubq, scanning electron microscopy was used. Bacterial cells (2.4 x 108 cells/ml) were treated separately with 7 μg/ml of AgNP and AgNP-Ubq for 1 h, and centrifuged at 3000 rpm for 10 min. The pellets were washed with phosphate buffer three times and pre-fixed with 2.5% glutaraldehyde for 30 min. The pre-fixed cells were washed with buffer two times followed by re-suspension in buffer. About 2 to 4 μl of samples were taken on a carbon tape. The fixed cells were dried and gold-coated using ion sputter. The samples were observed on a FEI Sirion XL30FEG SEM under high voltage varying between 200 kV and 300 kV.

NMR Spectroscopy

All NMR data were recorded at 298 K on a BRUKER Avance NMR spectrometer operating at a ^{1}H resonance frequency of 800 Hz equipped with a cryogenically cooled triple resonance probe. Chemical shifts were calibrated with respect to 2,2-dimethyl-2-silapentane-5-sulfonate (DSS) (0 ppm) for proton, while ^{15}N chemical shifts were calibrated indirectly. Ubiquitin concentration in all the experiments were kept at 50 μM in 50 mM Phosphate buffer, 50 mM KCl, pH 8 in a mixed solvent of 90% H_2O and 10% $^{2}H_2O$. The titration with AgNP was carried out by adding small aliquots from a stock solution to 500 μL of 34 nM dissolved in buffer with citrate as capping agent. Three samples were prepared by adding 100, 200 and 300 μl AgNP stock to 50 μM of ubiquitin and was equilibrated for 1 day each prior to NMR measurement. Since a low protein concentration was used, efficient fast data acquisition was enabled using SOFAST (band-Selective Optimized-Flip-Angle Short-Transient) HSQC[37] which has a combined advantage of: (i) small number of radio-frequency pulses, (ii) Ernst-angle excitation[38] and longitudinal relaxation optimization[39, 40] to perform the experiment with high repetition rate in order to achieve high signal to noise ratio using a small inter-scan delay period. The 2D [^{15}N, ^{1}H]-SOFAST-HMQC was recorded with

the ^{1}H carrier placed at middle of amide region (8.5 ppm) and with the ^{15}N carrier at 119 ppm. Selective excitation in amide region was achieved with a 1200 polychromatic pulse with 2.25 ms delay and for inversion R-SNOB pulse was used. The experimental time for each of the HMQC spectrum was 11 min with 128 × 2048 complex points along the ^{15}N and ^{1}H dimensions, respectively.

We performed HETerogeneity-SOFAST (HET-SOFAST) experiment to probe the change in structural rigidness of ubiquitin in residue wise manner due to interaction with AgNP[41]. In this direction, aliphatic region was two experiments in the presence (irradiation) and absence (reference) of a selective inversion pulse at desired offset (-1 ppm) were performed. Ratio of intensities for each peak leads to detection of λ_{noe} in a residue specific manner. The contribution of transverse relaxation in residue specific manner was obtained by incorporating a refocusing delay of 20 ms while the proton magnetization resides in XY plane and the intensity ratio was taken with and without this delay. Quadrature detection in the indirect dimension was achieved using States-TPPI method. All data were zero-filled to 1024 and 2096 complex points along t_1 and t_2, respectively. NMR data were apodized using 90°-shifted sine square bell window functions prior to Fourier Transform (FT) for attaining high resolution. The final size of each matrix was 2048(ω_2) × 1024 (ω_1). Residue-specific λ_{ex} values were determined by taking the intensity ratio $I_{excited}/I_{reference}$ for each cross-peak and in this case water saturation was achieved on selective inversion on water by putting a Gaussian pulse. All data were processed using TOPSPIN 3.2 and analysed using CARA.

The calculation of the dissociation constant, K_D, was carried out as follows. First, the number of protein molecules binding one AgNP particle was calculated using the equation[33].

$$n_{ubq} = 0.65*(R^3_{AgNP-Ubq} - R^3_{AgNP}) / R^3_{Ubq} \quad (1)$$

which is an upper limit on the number of ubiquitin molecules bound. 'R' denotes the radius of the nanoparticle/protein. Next, we assumed that all the binding sites on AgNP are independent of each other and the binding of ubiquitin to one site does not affect its binding to the other site on the AgNP surface. The dissociation constant (K_D) was then obtained by fitting Equation 2 below to the chemical shift data obtained from the titration experiment, which is valid for fast exchange and for a system with multiple binding sites for the ligand[42]. Here the protein represents the ligand and AgNP represents the macromolecule on which binding takes place:

$$\delta_{obs}-\delta_{free} = (\delta_{max})*[(n_{ubq}*[AgNP]_{total} + [Ubq]_{total} + K_D) - ((n_{ubq}*[AgNP]_{total} + [Ubq]_{total} + K_D)^2 - (4*n_{ubq}*[AgNP]_{total}*[Ubq]_{total})1/2)]/2*[Ubq]_{total} \quad (2)$$

Where $\delta_{max}=\delta_{bound} - \delta_{free}$ and δ_{obs}, δ_{free} are the chemical shifts of amide proton of a given residue of ubiquitin observed in the 2D [^{15}N, ^{1}H] HMQC in the presence and absence of AgNP, respectively; $[AgNP]_{total}$ and $[Ubq]_{total}$ represents the total concentration of AgNP and ubiquitin at a given point during the titration.

The amide proton T2 was determined by acquiring two 2D [^{15}N, ^{1}H] HSQC spectra on both the free AgNP and AgNP-Ubq complex. In one spectra, a delay period of 16 ms (T_{delay}) was added during the ^{1}H to ^{15}N polarization transfer step (i.e., during forward INEPT); the second spectra was acquired without any additional delay period. Assuming all other conditions identical, the ratio of the intensity for a given cross peak in the two spectra for a given sample (i.e., AgNP or AgNP-Ubq) is given as:

$$I_{delay}/I_{no\text{-}delay}=\exp(-T_{delay}/T_2(1H)) \quad (3)$$

Using the above relation, an estimate of the T2 can be obtained.

Results

Characterization of AgNP and AgNP-ubiquitin complex

The direct interaction of AgNPs with human ubquitin (Ubq) was first confirmed by UV-visible spectroscopy. The UV-visible spectrum of free (citrate capped) AgNP shows a typical intense surface plasmon resonance band positioned at 391 nm. Upon addition of Ubq this band shifts to 404 nm (Figure 1). The observed red shift is attributed to the formation of ubiquitin conjugated silver nanoparticles (AgNP-Ubq) as observed earlier[29]. The average particle size of the synthesized citrate capped AgNPs was found to be 25-30 nm from TEM. The TEM images of the AgNPs and AgNP-Ubq (Figure 1) show that the silver nanoparticles do not aggregate and remain monodispersed even in the presence of ubiquitin.

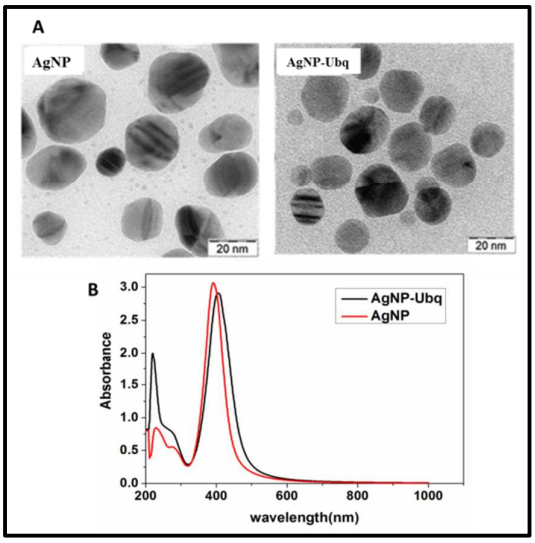

Figure 1 (A) TEM images (B) UV-visible spectra of AgNP and AgNP-Ubq

The hydrodynamic radii of AgNPs and AgNP-Ubq (at pH 7) obtained using DLS were found to be 31 nm and 36 nm, respectively. The higher hydrodynamic size of AgNP-Ubq as compared AgNPs suggests the formation of a complex of AgNP with ubiquitin. Figure 2A shows the zeta potential values of both unconjugated AgNPs and AgNP-Ubq complex at different pH values. For pH=3 to 11 (50 mM Phosphate buffer; 50 mM NaCl), the unconjugated AgNPs exhibit a negative zeta potential which decreases (in magnitude) upon forming complex with Ubq. At the corresponding pH values ubiquitin has both positively charged surface and negatively charged surfaces (Figure 2B), which was calculated based on the three dimensional structure of ubiquitin (PDB code 1UBQ). This suggests that the negative charge of the citrate capped AgNP is partially neutralized upon interaction with the positively charged surface of ubiquitin, resulting in the decrease (i.e., relatively more positive value) of the zeta potential. The fact that the positively charged surface of ubiquitin interacts with the AgNP was also verified from NMR studies (discussed below).

At pH ≤ 4, the AgNP-Ubq complex exhibits a positive zeta potential due to the fact that the overall surface of ubiquitin acquires relatively more positive charge compared to the pH > 4 (Figure 2B). In fact at pH 4 and 5 the AgNP-Ubq complex starts to become relatively unstable, though remaining more stable than the unconjugated AgNPs. This is discussed next.

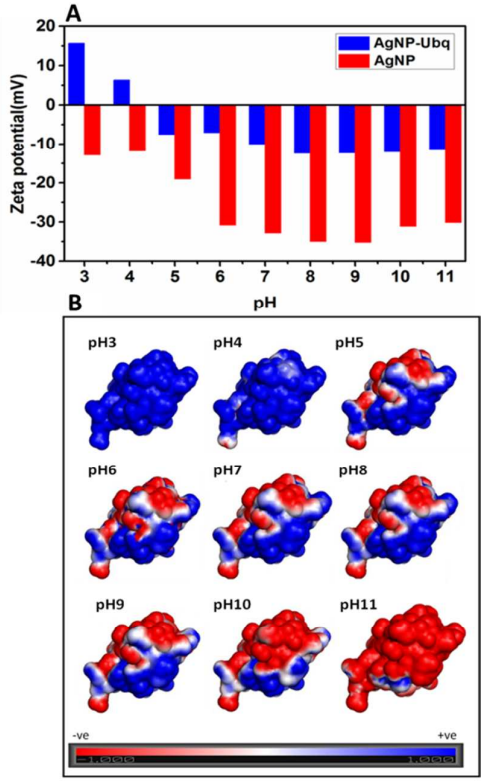

Figure 2. (A) Zeta potentials of AgNP and AgNP ubq conjugates at pH 3-11.(B) Electrostatic potential surface of ubiquitin at different pH, calculated using APBS server.

Stability of AgNPs and AgNP-Ubq complex

The stability of AgNPs and AgNP-Ubq were monitored by UV-visible spectroscopy over a period of several weeks. Figure 3A shows the absorbance profile of AgNPs (at λmax of 391 nm; shown in red) and that of AgNP-Ubq (blue) at λ_{max} of 404 nm as a function of time (in days) normalized with respect to the absorbance observed on day 0. The complete UV spectra at different pH is shown in Figure S1 of Supporting Information. A large decrease in absorbance of uncomplexed AgNPs is observed, corresponding to the loss of colour. Citrate capped AgNPs were unstable and underwent aggregation within a day at pH 4, 5, 6 and 10 (Figure S1); their stability was slightly higher at higher pH=7, 8 and 9. Surprisingly in presence of ubiquitin, AgNPs were stable for several weeks over a wide pH range. Indeed the AgNP-Ubq complex is stable even after 120 days (Figure 3B) as evident from its colour. At pH 4 and 5, AgNP-Ubq remained stable for two weeks, whereas the uncomplexed AgNPs degraded within a day. The mechanism resulting in such ultrahigh stability of the conjugate was investigated further by NMR spectroscopy.

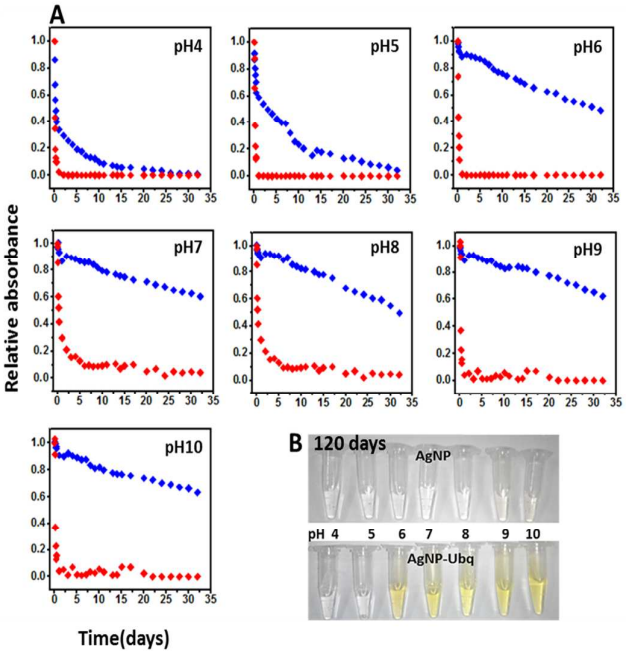

Figure 3. (A) Stability profiles of AgNPs (red) and AgNP-Ubq (blue) monitored by UV-visible spectroscopy as a function of time at different pH (pH=4 to10). The relative normalized absorbance at λ_{max} (391 nm for AgNP and 404 nm for AgNP-Ubq) has been plotted as a function of time (in days). (B) AgNP and AgNP-Ubq conjugates at different pH after 120 days.

NMR Studies of AgNP-ubiquitin interactions

(a) Characterizing the binding kinetics

We used different NMR techniques for probing the mechanistic aspects of AgNP-Ubq interactions. This was first studied with a fast two-dimensional (2D) ^{15}N-^{1}H heteronuclear multiple quantum coherence (HMQC) experiment[37] using a ^{15}N labeled sample of ubiquitin and titrating it with the AgNPs. Such a titration gives rise to chemical shift perturbations (CSP) of signals of the free (unbound) protein upon interaction with the AgNPs. CSP is a well known method for probing protein-ligand interactions[42]. Depending on the rate of exchange and the difference in chemical shift between the ubiquitin bound to AgNP and free ubiquitin, the kinetics of AgNP-Ubq interaction can be either designated as "slow" or "fast". In the slow exchange regime, the rate of exchange, k_{ex}, measured in Hz or s^{-1} would be less than the difference in the chemical shift (when considered in Hz) between the free and bound ubiquitin [40,43]. In the fast exchange regime, the exchange rate should be considerably high compared to the chemical shift difference between the free and bound ubiquitin. These two regimes can be identified from the NMR spectrum when the protein is titrated with the ligand. If the signals from the free protein gradually decrease in intensity with the concomitant appearance of signals at a location distinct from the original position, a slow exchange is implied. On the other hand, if the signals of the free protein gradually shift upon addition of the ligand, a fast chemical exchange can be inferred. The gradual shift in the signals occurs due to the increase in the population of the protein-ligand complex and the signals shift to a population weighted average position[42]. Further, in the fast exchange limit, the signals of the protein broaden which is manifested as a decrease in the intensity of peaks upon gradual addition of the ligand. This is due to the fact that fast exchange results in a population weighted average for the transverse relaxation times (T_2), which shifts to a value of the complex as more ligand is added. The average T_2 is significantly reduced if the protein-ligand complex is larger in size compared to the free protein. In the present study, the protein is ~2-3 nm in size compared to the AgNP which is ~30 nm resulting in a large AgNP-ubiquitin complex and consequently a very short T_2 is expected for the complex. Indeed the protein signals of AgNP-ubiquitin complex can be assumed to be completely broadened and unobservable due to its large size.

In the present study, we carried out two types of titrations. First, a 50 μM solution of ^{15}N labeled ubiquitin in 50 mM phosphate buffer (pH=8) in NMR tube was titrated with AgNPs taken from a stock solution of 34 nM made in the same buffer. The AgNPs were incrementally added to the solution and changes in chemical shifts and signal intensities in the 2D HMQC were observed. The NMR spectra were recorded for three additions of the nanoparticles taken from the stock solution of 34 nM: 100 μL, 200 μL and 300 μL. The titration were stopped when a significant broadening of peaks was observed in the 2D spectrum. We denote this as a 'forward' titration.

The second was a 'reverse' titration in which a fresh solution of 34 nm AgNPs was taken in the NMR tube and ^{15}N labeled ubiquitin was gradually added to it from a stock solution containing 5 mM of the protein. Three additions of the protein were carried out corresponding to the following concentrations: 50 μM, 200 μM and 500 μM. Due to fast exchange, a direct fit of intensity to the AgNP concentration could not be used to estimate the number of ubiquitin molecules binding one AgNP. Hence, given the size of ~30 nm for AgNP and ~36 nm for AgNP-Ubq complex as obtained from DLS at pH=8, we estimated that about ~800 molecules of ubiquitin were bound to one AgNP using the method proposed by Calzolai et al.[33] (see Equation 1 of Materials and Methods). Thus, in calculating the protein: AgNP ratio, the concentration of AgNP is scaled by 800 to compare it with the protein concentration. Taking this and the dilution of the solution during titration into consideration the forward titration points correspond to ~1:0.1, ~1:0.2 and ~1:0.3 protein: AgNP ratio. The reverse titration points correspond to: ~1:0.55, ~1:0.12 and ~1: 0.05 protein:AgNP ratio.

Figure 4A shows the 2D ^{15}N-^{1}H correlation spectrum of free ubiquitin overlayed with that of the protein titrated with AgNP corresponding to 1:0.3 ubiquitin:AgNP ratio. The fact that the overall chemical shifts of the complex are similar to that of the free protein indicates that the latter retains its backbone conformation in the bound form. However, subtle changes in the conformation is not reflected in the 2D spectrum, which was investigated in detail using other NMR techniques discussed below. Figure 4B shows the residues that are broadening at 1:0.3 Ubq:AgNP ratio mapped onto the surface of the protein. Figure 4C shows the deviation of the chemical shifts from the free form plotted for all residues at protein:AgNP ratio of 1:0.3. The gradual change in chemical shifts of some of the residues upon addition of the AgNP (reverse titration) compared to that in the unbound protein are shown in Figure 4D. This implies a fast exchange limit as discussed above. The proton (^{1}H) T_2 of the system compared to the unbound protein also decreases upon addition of AgNPs at different protein:AgNP ratios from 0.9±0.2 at 1: 0.1 to 0.4±0.1 at 1:0.3 ratio. As discussed above, this decrease in T_2 (^{1}H) with addition of the AgNPs also indicates a fast exchange regime. Figure 4E shows the average deviation plotted as a function of AgNP:protein ratio. From the change in the chemical shift as a function of protein:AgNP ratio the dissociation constant (K_D; indicative of the binding affinity) can be calculated using Equation 2 (see Materials and Methods). Assuming that 800 molecules of ubiquitin bind one AgNP (which is an upper limit on the number of ubiquitin molecules bound), we have considered 800 independent protein binding sites on AgNP (i.e., n_{ubq}=800 in Equation 2). A K_D of ~55±10 μM was obtained using this approach.

Journal Name

ARTICLE

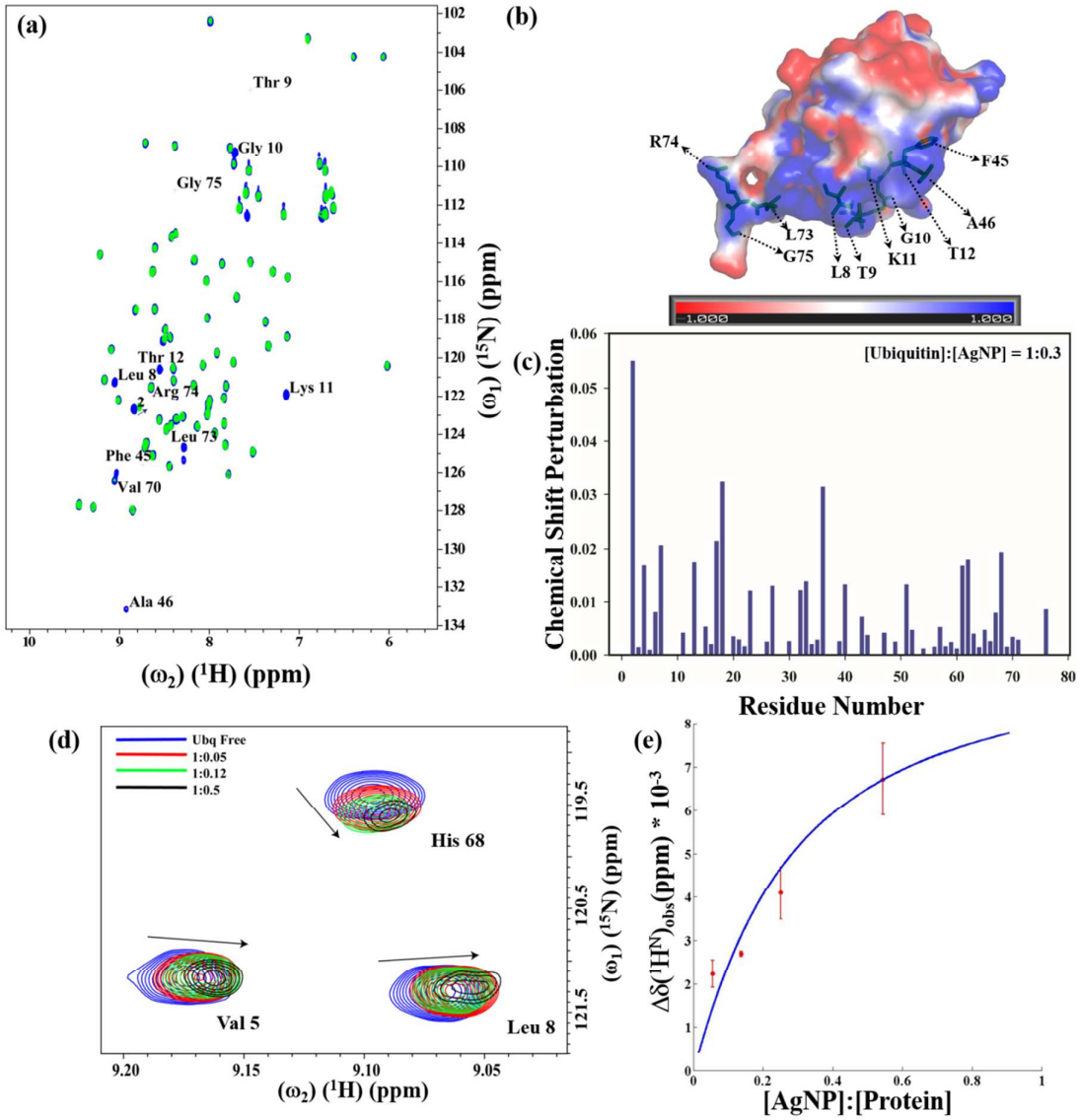

Figure 4: (A) Overlay of free (blue) ubiquitin and AgNP-Ubq (green) at a protein:AgNP ratio of 1:0.3. Residues that undergo broadening are labeled. Residue 2 undergoes a major change in its chemical shift in the bound form as indicated by the arrow. (B) The residues broadened out upon interaction with AgNP are mapped on the electrostatic surface of the protein. The sidechain of these residues are depicted using a stick model. The positively charged surface of the protein is shown in blue and the negatively charged surface in red colour. (c) Chemical Shift Perturbation (CSP) between free and bound form (at ubiquitin:AgNP ratio of 1:0.3) plotted in a residue wise manner. The chemical shift perturbation values were calculated using: $\sqrt{\{(\Delta(\delta_{1H})^2 + 0.14(\Delta\delta_{15N})^2\}}$ [33, 42], where $\Delta(\delta_{1H})$ and $\Delta(\delta_{15N})$ represent the difference in backbone ^{1}H and ^{15}N chemical shifts of ubiquitin between free and bound form. (d) Overlay of three residues at different protein:AgNP ratio from the reverse titration. (e) A plot of change in ^{1}H chemical shifts of a few residues at different AgNP:Protein ratios. The curve represents a fit of the observed changes to Equation 2 (See Methods and Materials) for estimation of the dissociation constant, K_D.

The maximum chemical shift difference observed for the bound form (complex) compared to the protein is estimated as $\Delta\delta_{max}$(ppm) ~ 0.03 by extrapolating the curve shown in Figure 4E to high protein:AgNP ratio. This corresponds to $\Delta\delta_{max}$ ~ 25 Hz at ^{1}H resonance frequency of 800 MHz at which the present studies were carried out. The fast exchange condition implies that the rate of exchange, k_{ex} (k_{off}) >> $\Delta\delta_{max}$ [42,43]. This implies a residence time ($1/k_{off}$) of much less than 40 ms, which is the upper limit based on the fast exchange considerations. The protein thus transiently contacts the AgNP and undergoes fast and reversible association-dissociation from the surface of AgNP. The implications of this for the stability of the nanoparticles is discussed below.

(b) Mapping the protein binding site

We found that a few residues of ubiquitin broaden out upon addition of AgNP at a protein:AgNP ratio of 1:0.3 (Figure 4A). The residues that get broadened are presumably those which transiently contact the citrate coated charged nanoparticle-surface and get broadened due to direct interaction. Specifically, these residues are Leu 8, Thr 9, Gly 10, Lys 11, Thr 12, Phe 45, Ala 46, Val 70, Leu 73, Arg 74, and Gly 75 (indicated in Figure 4A). When mapped upon the surface of ubiquitin (Figure 4B), the residues form distinct patches indicating different regions of protein that interact with the citrate coated surface of AgNP. This is similar to that observed recently for the interaction of ubiquitin with gold nanoparticles [44]. Interestingly these residues are located in the positively charged surface of ubiquitin as shown in Figure 4B. We have used implicit solvent methods [45, 46] to calculate the electrostatic potential on the protein structure considering solvent as a dielectric continuum and using APBS (Adaptive Poisson-Boltzmann Solver) [47] in PYMOL [48] together with a web-based service [49] provided at http://www.poissonboltzmann.org/. This establishes the fact that AgNP-Ubq interaction is largely electrostatic in nature and residues which belongs to positively charged surface favor the binding to negatively charged citrate capped AgNPs.

(c) Conformational changes in ubiquitin upon binding AgNP

In order to understand further the protein-nanoparticle interaction, we performed detailed analysis of local conformational fluctuations of ubiquitin using NMR based relaxation experiments. Two distinct types of experiments were preformed, both of which have been described by Schanda et al. [41]. In the first case, aliphatic (methyl) protons were saturated using a selective radio frequency (r.f.) pulse prior to recording a 2D ^{15}N, ^{1}H correlation experiment and the saturation transfer to backbone amide protons was monitored by taking the integral ratio (λ_{noe}) of two spectra recorded with (saturated) and without (reference) selective irradiation of the aliphatic region[41]. The primary mechanism of transfer of magnetization from aliphatic to backbone amide is spin diffusion; the ratio measured provides insight into the interaction between the backbone amide protons and aliphatic proton and leads to nuclear Overhausser effect (NOE) information (λ_{noe}). When a backbone amide hydrogen atom is located in the interior of a structured protein, we observe a low value of λ_{noe} due to efficient spin diffusion mechanism arising from its close proximity (< 5Å) to other protons. Hence, an increase in λ_{noe} corresponds to loosening in structure or increase in the mobility of the amides upon forming the complex. This was probed for both the free (unbound) protein and the protein in complex with AgNP at protein:AgNP ratio of 1:0.3.

In the second experiment an estimation of the amide–water hydrogen exchange (λ_{ex}) was obtained using the same procedure as above except that the selective ^{1}H saturation was carried out for the water signal (at 4.7 ppm). The ratio of peak integrals of two spectra recorded with (saturation) and without (reference) selective irradiation of the water peak is denoted as: λ_{ex}. A value of λ_{ex} close to 1.0 indicates that the amide protein is protected from the solvent and hence irradiation of the water signal does not affect its intensity. A lower value of λ_{ex} implies exposure to the solvent resulting from its higher exchange with the solvent, which causes its intensity to decrease due to saturation transfer[41]. Thus the two parameters (λ_{noe} and λ_{ex}) reveal local structural and dynamics information along polypeptide chain and are complementary in nature.

Journal Name

ARTICLE

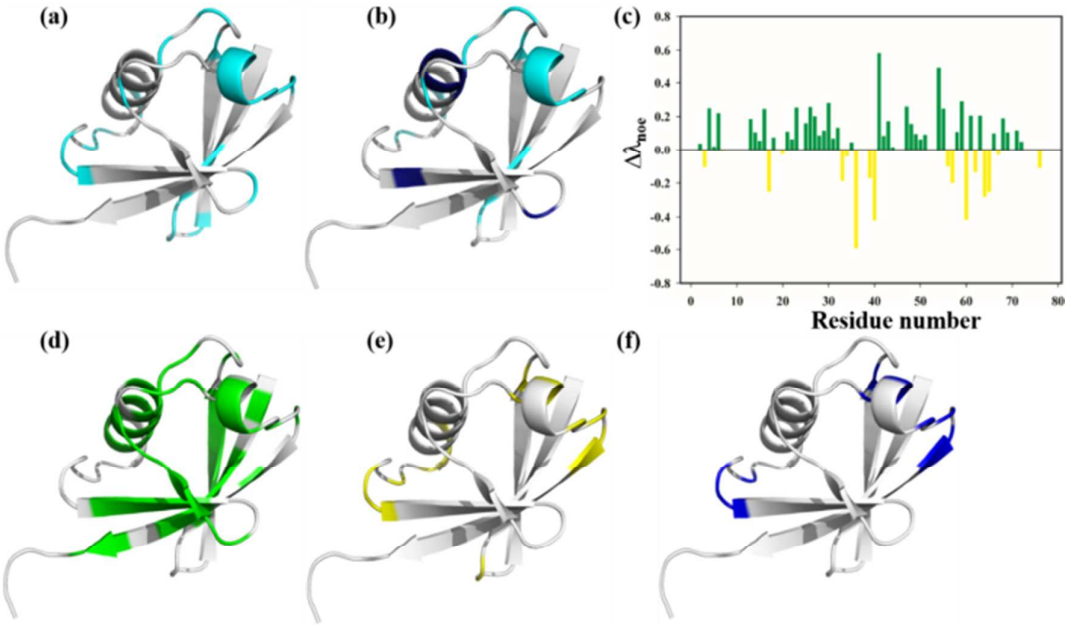

Figure 5: Residues in (a) free ubiquitin and (b) AgNP-Ubq that exhibit $\lambda_{noe} > 0.7$ shown mapped on to the 3D structure. In (b), residues in AgNP-Ubq which additionally have $\lambda_{noe} > 0.7$ compared to free ubiquitin are shown in a different color (pink). (c) Difference in λ_{noe} between bound (AgNP-Ubq) and free ubiquitin plotted as a function of residue. (d) Residues which show increase in λ_{noe} values upon interaction with AgNP (i.e., $\Delta\lambda_{noe} > 0$). (e) Residues with $\Delta\lambda_{noe} < 0$ and (f) residues which show decrease in T2 (^{1}H) upon interaction with AgNP are mapped on the structure of the protein.

Figure 5A shows residues in the free form of the protein that have high λ_{noe} (> 0.7) mapped on the 3D structure of the protein. A majority of these are distributed over loops, at the edges of secondary structural elements and/or exposed to the solvent. We have considered a cut-off value of 0.7 for λ_{noe}, which is 1.3 times the average value for the protein to discriminate the flexible residues from the rest of the protein. Upon interaction with AgNP, the overall conformation of ubiquitin starts opening up as more residues show higher flexibility and λ_{noe} values. These are distributed over different parts of the structure as shown in Figure 5B, where the additional residues showing higher λ_{noe} values (considering a similar cut-off as used for the free form) are shown in pink and correspond to Lys 11, Asp 16, Thr 22-Val 26, Lys 29, Ile 30, Gln 41, Gly 47, Arg 54, Thr 55, Lys 63, and Leu 73. A difference of the λ_{noe} values in the bound and free form ($\Delta\lambda_{noe}$) is shown in Figure 5C. The residues which show increase in λ_{noe} upon interaction (i.e., $\Delta\lambda_{noe} > 0$) are shown in Figure 5D mapped onto the protein structure and are more in number compared to those with $\Delta\lambda_{noe} < 0$.

The residues with $\Delta\lambda_{noe} < 0$ are shown in Figure 5E and correspond to Val 17, Lys 33, Glu 34, Ile 36, Asp 39, Gln 40, Leu 56, Ser 57, Asn 60, Gln 62, Glu 64, Ser 65. Some of these residues are located in loops and at edges of the secondary structural elements and in vicinity of residues involved in direct interaction with AgNP (see Figure 4B). Additionally Asn 60-Ser 65 belonging to the flexible loop before the C-terminal β-sheet of ubiquitin also show increase in rigidity upon interaction (i.e., $\Delta\lambda_{noe} < 0$). These residues are located in the vicinity of Val 70 belonging to the C-terminal β-sheet and the residues at the C-terminal end (Leu 73, Arg 74 and Gly 75), which are involved in direct interaction with AgNP surface and are broadened out (Figure 4A). To further confirm that this decrease in λ_{noe} is mainly due to decrease in local flexibility, we estimated transverse relaxation (T_2) of backbone amide protons. We have found that most of the residues which show decrease in λ_{noe} also show decrease in T_2 (Val 17, Ile 36, Asp 39, Gln 40, Leu 56, Ser 57, Asn 60, Gln 62, Glu 64, Ser 65, Gly 76) upon interacting with AgNP. This is shown in Figure 5F and Figure S2 of Supporting Information.

The overall opening up of the conformation is also reflected in the increase in the solvent (water) accessibility of the amide proton for some of the residues (Figure S3 of Supporting Information). For instance, in the free protein the residues Lys 11, Ser 20, Gly 47, and Gln 62, which show high

solvent accessibility are located largely in the flexible loop regions of the structure. However upon interaction with AgNP, residues Val 5, Lys 6, Thr 7, Thr 14, Thr 22, Ile 23, Ile 30, Lys 33, Gly 47, Asp 52, Tyr 59, Ile 61, Glu 64 and Val 70 show higher accessibility (Figure S3). These residues are located in vicinity of those that show higher λ_{noe} values.

Taken together, the above results suggest the following mechanism: the positively charged surface of ubiquitin makes transient contacts with the negatively charged citrate coated AgNP surface. Upon interaction the protein readjusts its conformation in two ways: (i) reducing the mobility of residues in vicinity of the binding site and (ii) an overall loosening or opening of the structure presumably to attain a more thermodynamically favorable energy upon binding. An increase in rigidity upon binding to AgNP ($\Delta\lambda_{noe} < 0$) for residues located in loops and at edges of the secondary structural elements results possibly from their reduced conformational exchange upon interaction.

E. coli cells treated with AgNPs and AgNPs-Ubq complex

As an application of the ultrastable AgNP-Ubq conjugate, we carried out an anti-bacterial test. The morphological changes of *E. coli* cells upon treatment with AgNP and AgNP-Ubq complex were observed by SEM (Figure 6). The untreated (control) cells were typically cylindrical rod-shaped. There was no damage or any destruction observed on any of cell surface. However, in the AgNPs and AgNP-Ubq treated groups, we observed ruptured cell wall and cell fragments arising from damage to the cell membrane. This is similar to that observed in bacterial cells treated with silver nanoparticles[50]. Bactericidal activity of AgNP and AgNP-Ubq were also studied by monitoring the bacterial growth kinetics at different time points and under different concentrations (shown in Figure S4 of Supporting Information).

While both AgNP and AgNP-Ubq affected the growth kinetics equally as compared to the negative control (culture grown in absence of antimicrobial agent) the fate of AgNPs and AgNP-Ubq after one hour of exposure to the culture medium containing *E. coli* cells was very different. This was monitored by recovering the nanoparticles and the conjugate and characterizing them by TEM and UV-visible spectroscopy. The recovered AgNPs (denoted as R-AgNP) exhibited aggregation to form large clusters as depicted in Figure 6. This was is reflected in the UV-visible spectra of recovered AgNPs wherein the characteristic absorption maxima at 391 appears broadened with an additional shoulder peak at a higher wavelength, which is attributed to the formation of larger nanoparticle aggregates[30]. On the other hand, the recovered AgNP-Ubq complex (denoted as R-AgNP-Ubq) remained mono dispersed with intact shapes as seen in the TEM images (Figure 6B). The conjugate also retained its characteristic absorption maxima at 404 nm as observed in the UV-visible spectrum (Figure 6C). This implies that the AgNP-Ubq complex can be re-cycled for use repeatedly compared to the unconjugated AgNP, which makes them more efficient as anti-bacterial agents.

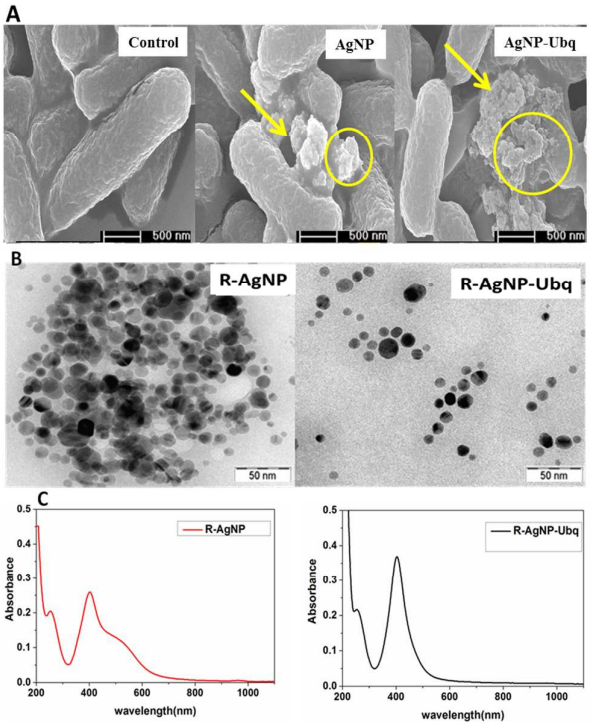

Figure 6 (A) SEM images of untreated (control) *E. coli* cells and those treated with AgNP and AgNP-Ubq. The cell rupture and damage is highlighted and arises due to the antimicrobial action of AgNPs (B) TEM images of recovered (R-) AgNPs and R-AgNP-Ubq. R-AgNP nanoparticle tend to aggregate where as R-AgNP-Ubq complex remained mono dispersed particles with intact spherical shape. (C) UV-visible spectra of recovered AgNPs and AgNP-Ubq. UV-visible spectra of recovered AgNPs broadened whereas AgNP-Ubq retained its characteristic absorption maxima (see Figure 1).

Discussion

The stability of nanoparticles in general and silver nanoparticles in particular is pivotal for various applications [51-53]. The present study brings out for the first time several features of protein-AgNP interactions: (i) the conjugate of AgNP with ubiquitin is highly stable over a wide pH range compared to unconjugated AgNPs, (ii) ubiquitin interacts with AgNP through electrostatic interactions and undergoes a dynamic exchange at a rate much faster than 25 s^{-1} and reversible association (adsorption) with a dissociation constant of ~55 μM and (iii) there are subtle conformational changes in ubiquitin upon interaction. The stability of the AgNP-Ubq conjugate can be understood by considering both the electrostatic and steric contributions to stability. The stability of colloids is a balance between the attractive van der Waals' forces between the nanoparticles and electrostatic repulsion because of their net surface charge or due to bulky groups on the surface that prevent the nanoparticles to come closer [54-56]. The ultrastability of AgNP-Ubq as observed in the present study is attributed to a combination of both electrostatic as well as steric stabilization, which is also termed as 'electrosteric' stabilization [57]. A mechanism involving a combination of these interactions together with weak anchoring of the macromolecule has been described

previously for colloidal particles[58]. A detailed calculation of the energy of the system, which consists of attractive, electrostatic repulsive and steric interactions is described in the Supporting Information (Text S1 and Figure S5). The dynamic and reversible association-dissociation of ubiquitin molecules ensure that the AgNP surface is always adsorbed with the protein molecules, provided the latter are in excess. Interestingly, ubiquitin has two oppositely charged surfaces (Figures 2 and 4). The positively charged region is attracted to the negatively charged citrate capped surface of AgNP. On the other hand, the negatively charged surface of ubiquitin points to the solvent and prevents aggregation by both electrostatic and steric repulsion.

The stability of protein-nanoparticle conjugates has been reported previously for different nanoparticles [29, 33, 34]. We discuss two recently reported studies on stability of protein-nanoparticle interactions revealing similar mechanisms as discussed here. In one study, silica nanoparticles were first coated with negatively charged linker molecules on the surface of the particles[59]. Following this, the nanoparticles were conjugated with anti-bodies which were attracted to the negatively charged surface by electrostatic interaction. The antibody-nanoparticle complex formed remained monodisperse presumably due to steric stabilization. In another study, the protein Bovine Serum Albumin (BSA) was conjugated with silver nanoparticles under acidic conditions and the stability of the resulting complex was attributed to steric repulsion [60]. The conjugates remained stable for a few days at lower pH (< 7) in contrast to stability at higher pH that we have observed. The higher stability presumably arises from steric repulsion. Interestingly, the size of the AgNPs used were similar to that used in our study (ca. 25 nm) and the binding affinity estimated for the AgNP-protein conjugate was $K_D \approx 1$ μM. Our study thus brings out the mechanism which may be valid for protein-nanoparticle interactions in general. A more detailed insight into the thermodynamic aspects of the dynamic interactions and stabilization remains to be explored.

Conclusion

In summary, our studies reveal for the first time a conjugate of protein with silver nanoparticles which remains stable for months over a wide pH range through a mechanism involving structural and dynamic interaction of the protein with the nanoparticles. The protein molecules transiently adsorb on the negatively charged surface of the AgNP by electrostatic interactions and undergo conformational changes. The fast exchange (adsorption-dissociation) happens at the rate >> 25 s^{-1}. The conjugate is rendered ultrastable by a combination of both electrostatic and steric interactions, with the latter playing a dominant role. Taken together, the study opens up new avenues for application of such stable protein-nanoparticle conjugates in a wide range of systems.

Acknowledgements

The facilities provided by NMR Research Centre at IISc and Research Grants supported by Department of Science and Technology (DST), India is gratefully acknowledged. KC acknowledges support from DST-INSPIRE research grant. We thank Ravula Thirupathi for helping in preparing the figures and Soumya for help in obtaining the DLS and Zeta-potential data.

Notes and references

1. M. Mashayekh and D. Dorranian, *Optik - International Journal for Light and Electron Optics*, 2014, **125**, 5612-5617.
2. P. A. Tran, D. M. Hocking and A. J. O'Connor, *Materials Science and Engineering: C*, 2015, **47**, 63-69.
3. C.-H. Xue, J. Chen, W. Yin, S.-T. Jia and J.-Z. Ma, *Applied Surface Science*, 2012, **258**, 2468-2472.
4. A. Haider and I.-K. Kang, *Advances in Materials Science and Engineering*, 2015, **2015**, 16.
5. E. Abbasi, M. Milani, S. Fekri Aval, M. Kouhi, A. Akbarzadeh, H. Tayefi Nasrabadi, P. Nikasa, S. W. Joo, Y. Hanifehpour, K. Nejati-Koshki and M. Samiei, *Critical reviews in microbiology*, 2014, DOI: 10.3109/1040841x.2014.912200, 1-8.
6. H. Ki, J. Kim, S. Kwon and S. Jeong, *Journal of Material Science*, 2007, **42**, 8020-8024.
7. F. Zhang, X. Wu, Y. Chen and H. Lin, *Fibers and Polymers*, 2009, **10**, 496-501.
8. K. Chaloupka, Y. Malam and A. M. Seifalian, *Trends in Biotechnology*, 2010, **28**, 580-588.
9. M. Rai, A. Yadav and A. Gade, *Biotechnology advances*, 2009, **27**, 76-83.
10. J. Jain, S. Arora, J. M. Rajwade, P. Omray, S. Khandelwal and K. M. Paknikar, *Molecular pharmaceutics*, 2009, **6**, 1388-1401.
11. R. M. El-Shishtawy, A. M. Asiri and M. M. Al-Otaibi, *Spectrochimica acta. Part A, Molecular and Biomolecular Spectroscopy*, 2011, **79**, 1505-1510.
12. A. Desireddy, B. E. Conn, J. Guo, B. Yoon, R. N. Barnett, B. M. Monahan, K. Kirschbaum, W. P. Griffith, R. L. Whetten, U. Landman and T. P. Bigioni, *Nature*, 2013, **501**, 399-402.
13. A. Mari, P. Imperatori, G. Marchegiani, L. Pilloni, A. Mezzi, S. Kaciulis, C. Cannas, C. Meneghini, S. Mobilio and L. Suber, *Langmuir*, 2010, **26**, 15561-15566.
14. G. F. Prozorova, A. S. Pozdnyakov, N. P. Kuznetsova, S. A. Korzhova, A. I. Emel'yanov, T. G. Ermakova, T. y. V. Fadeeva and L. M. Sosedova, *International Journal of Nanomedicine*, 2014, **9**, 1883-1889.
15. L. Balogh, D. R. Swanson, D. A. Tomalia, G. L. Hagnauer and A. T. McManus, *Nano Letters*, 2000, **1**, 18-21.
16. V. Sambhy, M. M. MacBride, B. R. Peterson and A. Sen, *Journal of the American Chemical Society*, 2006, **128**, 9798-9808.
17. L. Yu, Y. Zhang, B. Zhang and J. Liu, *Scientific. Reports.*, 2014, **4,** DOI:10.1038/srep04551.
18. A. Kubacka, M. S. Diez, D. Rojo, R. Bargiela, S. Ciordia, I. Zapico, J. P. Albar, C. Barbas, V. A. P. Martins dos Santos,

M. Fernandez-Garcia and M. Ferrer, *Scientific. Reports*, 2014, **4,** DOI: 10.1038/srep04134.
19. A. Travan, E. Marsich, I. Donati, M. Benincasa, M. Giazzon, L. Felisari and S. Paoletti, *Acta Biomaterialia*, 2011, **7**, 337-346.
20. C. M. Pickart and M. J. Eddins, *Biochimica et Biophysica Acta*, 2004, **1695**, 55-72.
21. Y. Hou, J. Zhou, Z. Gao, X. Sun, C. Liu, D. Shangguan, W. Yang and M. Gao, *ACS Nano*, 2015, DOI: 10.1021/acsnano.5b00276.
22. T. K. Sau, A. L. Rogach, F. Jäckel, T. A. Klar and J. Feldmann, *Advanced Materials*, 2010, **22**, 1805-1825.
23. S. Tenzer, D. Docter, J. Kuharev, A. Musyanovych, V. Fetz, R. Hecht, F. Schlenk, D. Fischer, K. Kiouptsi, C. Reinhardt, K. Landfester, H. Schild, M. Maskos, S. K. Knauer and R. H. Stauber, *Nature Nanotechnology*, 2013, **8**, 772-781.
24. U. Sakulkhu, M. Mahmoudi, L. Maurizi, J. Salaklang and H. Hofmann, *Scientific. Reports.*, 2014, **4**, DOI: 10.1038/srep05020
25. A. E. Nel, L. Madler, D. Velegol, T. Xia, E. M. V. Hoek, P. Somasundaran, F. Klaessig, V. Castranova and M. Thompson, *Nature Materials*, 2009, **8**, 543-557.
26. J. Sund, H. Alenius, M. Vippola, K. Savolainen and A. Puustinen, *ACS Nano*, 2011, **5**, 4300-4309.
27. L. Wei, J. Lu, H. Xu, A. Patel, Z. S. Chen and G. Chen, *Drug DiscoveryToday*, 2014, DOI: 10.1016/j.drudis.2014.11.014.
28. D. Ballestero, R. Juan, A. Ibarra, C. Gómez-Giménez, C. Ruiz, B. Rubio and M. Teresa Izquierdo, *Colloids and Surfaces A: Physicochemical and Engineering Aspects*, 2015, **468**, 140-150.
29. F. Ding, S. Radic, R. Chen, P. Chen, N. K. Geitner, J. M. Brown and P. C. Ke, *Nanoscale*, 2013, **5**, 9162-9169.
30. O. Soltwedel, O. Ivanova, M. Höhne, M. Gopinadhan and C. A. Helm, *Langmuir*, 2010, **26**, 15219-15228.
31. O. Vinogradova and J. Qin, *Topics in current chemistry*, 2012, **326**, 35-45.
32. E. R. Zuiderweg, *Biochemistry*, 2002, **41**, 1-7.
33. L. Calzolai, F. Franchini, D. Gilliland and F. Rossi, *Nano Letters*, 2010, **10**, 3101-3105.
34. M. Lundqvist, I. Sethson and B. H. Jonsson, *Langmuir*, 2004, **20**, 10639-10647.
35. V. Mangini, M. Dell'Aglio, A. D. Stradis, A. D. Giacomo, O. D. Pascale, G. Natile and F. Arnesano, *Chemistry – A European Journal*, 2014, **20**, 10745-10751.
36. M. Assfalg, L. Ragona, K. Pagano, M. D'Onofrio, S. Zanzoni, S. Tomaselli and H. Molinari, *Biochimica et Biophysica Acta (BBA) - Proteins and Proteomics*, DOI: http://dx.doi.org/10.1016/j.bbapap.2015.04.024.
37. P. Schanda, E. Kupce and B. Brutscher, *Journal of Biomolecular NMR*, 2005, **33**, 199-211.
38. A. Ross, M. Salzmann and H. Senn, *Journal of Biomolecular NMR*, 1997, **10**, 389-396.
39. K. Pervushin, B. Vogeli and A. Eletsky, *Journal of the American Chemical Society*, 2002, **124**, 12898-12902.
40. H. S. Atreya and T. Szyperski, *Proceedings of the National Academy of Sciences of the United States of America*, 2004, **101**, 9642-9647.
41. P. Schanda, V. Forge and B. Brutscher, *Magnetic Resonance in Chemistry : MRC*, 2006, **44**, S177-184.
42. M. P. Williamson, *Progress in Nuclear Magnetic Resonance Spectroscopy*, 2013, **73**, 1-16.
43. A. D. Bain, *Progress in Nuclear Magnetic Resonance Spectroscopy*, 2003, **43**, 63-103.
44. G. Brancolini, D. B. Kokh, L. Calzolai, R. C. Wade and S. Corni, *Acs Nano*, 2012, **6**, 9863-9878.
45. P. Ren, J. Chun, D. G. Thomas, M. J. Schnieders, M. Marucho, J. Zhang and N. A. Baker, *Quarterly Reviews of Biophysics*, 2012, **45**, 427-491.
46. F. Dong, B. Olsen and N. A. Baker, in *Biophysical Tools for Biologists: Vol 1 in Vitro Techniques*, eds. J. J. Correia and H. W. Detrich, 2008, vol. 84, pp. 843-+.
47. N. A. Baker, D. Sept, S. Joseph, M. J. Holst and J. A. McCammon, *Proceedings of the National Academy of Sciences of the United States of America*, 2001, **98**, 10037-10041.
48. V. S. The PyMOL Molecular Graphics System, LLC.
49. S. Unni, Y. Huang, R. M. Hanson, M. Tobias, S. Krishnan, W. W. Li, J. E. Nielsen and N. A. Baker, *Journal of Computational Chemistry*, 2011, **32**, 1488-1491.
50. S. Agnihotri, S. Mukherji and S. Mukherji, *RSC Advances*, 2014, **4**, 3974-3983.
51. D. M. Eby, N. M. Schaeublin, K. E. Farrington, S. M. Hussain and G. R. Johnson, *ACS Nano*, 2009, **3**, 984-994.
52. A. Sooresh, H. Kwon, R. Taylor, P. Pietrantonio, M. Pine and C. M. Sayes, *ACS Applied Materials & Interfaces*, 2011, **3**, 3779-3787.
53. W. Shao, X. Liu, H. Min, G. Dong, Q. Feng and S. Zuo, *ACS Applied Materials & Interfaces*, 2015, **7**, 6966-6973.
54. H. Ohshima, in *Electrical Phenomena at Interfaces and Biointerfaces*, John Wiley & Sons, Inc., 2012, DOI: 10.1002/9781118135440.ch3, pp. 27-34.
55. L. L. B.Derjaguin, *Acta Physico Chemica URSS*, 1941, **14**, 633.
56. E. J. W. O. Verwey, J. Th. G, *Theory of the stability of lyophobic colloids*, Amsterdam: Elsevier, 1948.
57. M. Hoppe, R. Mikutta, J. Utermann, W. Duijnisveld and G. Guggenberger, *Environmental Science & Technology*, 2014, **48**, 12628-12635.
58. D. H. Napper and A. Netschey, *Journal of Colloid and Interface Science*, 1971, **37**, 528-535.
59. C. J. Moore, H. Monton, R. O'Kennedy, D. E. Williams, C. Nogues, C. Crean and V. Gubala, *Journal of Materials Chemistry B*, 2015, **3**, 2043-2055.
60. J.-T. Tai, C.-S. Lai, H.-C. Ho, Y.-S. Yeh, H.-F. Wang, R.-M. Ho and D.-H. Tsai, *Langmuir*, 2014, **30**, 12755-12764.